Breakdown of fast water transport in graphene oxides

Ning Wei,[1] Xinsheng Peng,[2] and Zhiping Xu[1,*]
[1]*Applied Mechanics Laboratory, Department of Engineering Mechanics, Center for Nano and Micro Mechanics, Tsinghua University, Beijing 100084, China*
[2]*Department of Materials Science and Engineering, State Key Laboratory of Silicon Materials, Zhejiang University, Hangzhou 310028, China*
(Received 16 July 2013; published 13 January 2014)

Fast slip flow was identified for water inside the interlayer gallery between graphene layers or carbon nanotubes. We report here that this significant flow rate enhancement (over two orders) breaks down with the presence of chemical functionalization and relaxation of nanoconfinement in graphene oxides. Molecular dynamics simulation results show that hydrodynamics applies in this circumstance, even at length scales down to nanometers. However, corrections to the slip boundary condition and apparent viscosity of nanoconfined flow must be included to make quantitative predictions. These results were discussed with the structural characteristics of liquid water and hydrogen-bond networks.

DOI: 10.1103/PhysRevE.89.012113 PACS number(s): 61.20.−p, 47.15.−x, 68.08.−p, 47.11.Mn

I. INTRODUCTION

Recent studies have revealed ultrafast fluid flow in hydrophobic nanoconfined environments, e.g., inside carbon nanotubes and interlayer gallery between graphene sheets [1–5]. The remarkably enhanced water transport deviates distinctly from the prediction using macroscopic viscous flow models and yet holds great promise in filtration and energy conversion applications [6]. The observation was explained mainly by referring to the low friction between the water and the graphitic surfaces where notable interfacial slip occurs [1–5,7–9]. The flow enhancement also was attributed to the modified water structures of water in the nanosized channel, which is a hallmark of a nanoconfined liquid [10,11]. A curvature-induced effect was reported in a comparative study between graphene and carbon nanotubes with different channel widths, and the slip length of the water flow in carbon nanotubes was found to decrease with its diameter towards the value for graphene [3]. "Structured water" was identified for flows inside carbon nanotubes with diameters less than 1.25 nm [12], including single-file chains, tilted, stacked pentagons, and hexagons. However, all these studies were conducted in nanochannels with atomistically smooth graphitic walls, and the critical effect from the atomistic roughness, such as those created by imperfections and chemical functionalization, was completely excluded [9]. In contrast, an exemplified study recently showed that, for water flow between graphene oxide (GO) sheets, an oxidized region prohibits fast water transport [13]. Instead, a two-dimensional (2D) network could form between the pristine graphene region in the GO sheets, still featuring significant flow enhancement, and a capillary-driven flow mechanism was proposed to explain the unusually high water permeance [13].

To clarify the roles of surface functionalization in combination with the nanoconfinement, we performed pressure-driven flow simulations to quantify the nature of interlayer flow between graphene and GO sheets, respectively. The structures of liquid water and hydrogen-bond (H-bond) networks between them that correlate with both functionalization and nanoconfinement were analyzed and were discussed. We find that a very low concentration (~5%) of hydroxyl groups on the graphene sheet reduces the slip length by 97% from 48.13 ± 4.02 to 1.26 ± 0.31 nm. The dependence of the flow rate on the pressure gradient follows the Poiseuille law for viscous flow only after corrections on the apparent viscosity and interfacial slip condition have been performed.

II. MODELS AND METHODS

The molecular structure of graphene oxides consists of hydroxyl, epoxy, and carbonyl groups on the basal plane, defective sites, and open edges where the hydroxyl groups were reported to be able to stay enriched in the long-living quasiequilibrium state [14]. A typical fraction of hydroxyl species relative to the amount of carbon atoms in GO is ~20% [14]. Further reduction could yield lower concentrations (13.9%–15.9%) in the reduced graphene oxide [15]. For simplicity, we constructed hydroxyl-functionalized graphene (on both sides of the sheet) with various concentrations c, defined as $c = n_{OH}/n_C$ (n_{OH} and n_C are the numbers of hydroxyl groups and carbon atoms, respectively). The distribution of hydroxyl groups was sampled randomly.

Classical molecular dynamics (MD) simulations were performed using the large-scale atomic/molecular massively parallel simulator (LAMMPS) [16]. The all-atom optimized potentials for liquid simulations (OPLS-AA) were used for GO, which are able to capture essential many-body terms in interatomic interactions, i.e., bond stretching, bond angle bending, and van der Waals and electrostatic interactions [17]. This potential was applied successfully in a study of the pH-dependent behavior of graphene oxide aqueous solutions and was compared to experimental results [17]. Following previous studies on similar systems, the rigid simple point charge effective pair (SPC/E) model for water molecules was used [3,18]. The SHAKE algorithm was applied for the stretching terms between oxygen and hydrogen atoms to reduce high-frequency vibrations that require shorter time steps. The interaction between water and GO includes both van der Waals and electrostatic terms. The former one was described by the

*xuzp@tsinghua.edu.cn

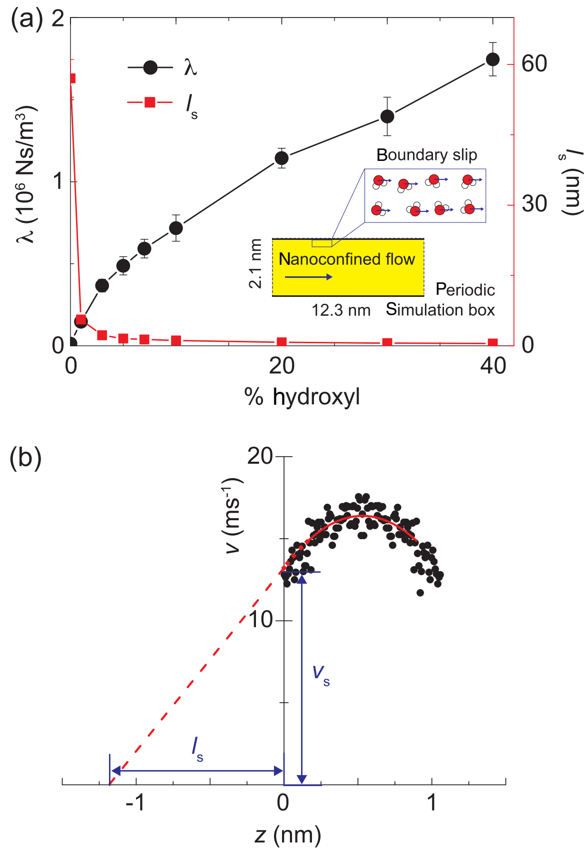

FIG. 1. (Color online) (a) Friction coefficient λ (black line and circles) and slip length l_s (red line and squares) as functions of the concentration of hydroxyl groups on the functionalized graphene sheet with interlayer distance $h = 1.7$ nm. The error bar of friction coefficients is plotted using their max or min values. (b) One example of the slip length determination in our paper. The solid red line is a parabolic fit to the simulation data, the extension of which from $z = 0$ intersects with the x axis at $-l_s$. The plane $z = 0$ is defined as the average position of the first water layer from the GO sheets.

12-6 Lennard-Jones potential $4\varepsilon[(\sigma/r)^{12} - (\sigma/r)^6]$ between oxygen and carbon atoms with parameters $\varepsilon = 4.063$ meV and $\sigma = 0.319$ nm at an interatomic distance r [19]. Periodic boundary conditions were applied on all directions [Fig. 1(a), inset]. The channel length along the flow (x) direction is 12.3 nm, and the width is 2.1 nm. In order to ensure that the channel is filled at 1 atm, we adjusted the interlayer distance accordingly at room temperature (300 K) for a specific number of atoms. For example, there are 529, 1136, and 2354 water molecules included for interlayer distance h of 1.0, 1.7, and 3.1 nm, respectively. Here h is the distance measured from basal planes in GO. As will be discussed later, the nature of flow strongly correlates with the liquid-solid interfacial properties, one of the key parameters for which the contact angle is θ_c. This set of parameters predicts a contact angle of 95°, inconsistent with the experimental measurement [20]. The van der Waals forces were truncated at 1.0 nm, and the long-range Coulomb interactions were computed by using the particle-particle particle-mesh algorithm [21]. To validate our model for GO, we further calculated the contact angle θ_c between the water and the graphene sheet with c up to 20%. The results show that θ_c decreases as c increases (e.g., $\theta_c = 29.1°$ at $c = 20\%$). This result is consistent with recent experimental measurement 33.7° [22] and validates the combined OPLS-AA and SPC/E approach, which here can yield a reasonable prediction for the water and GO hybrid system.

The pressure-driven water flow was simulated by directly applying forces to water molecules. This nonequilibrium molecular dynamics (NEMD) approach was widely used to explore fluid flow [18,23]. Attention must be paid in order that, for large slippage, as for water flow between pristine graphene, the NEMD method is not suitable since the quadratic fit of the flow velocity profile will be associated with a very large statistical uncertainty [5]. Rather wide channels must be constructed to identify the slip length in this situation. The validity of this method was assessed by comparison with additional simulations where forces were applied to water molecules in a specified region only, i.e., within a 2.1 nm block in the 12.3 nm long channel. The results we obtained show almost no difference for the velocity profile of the water flow between graphene sheets but deviation for the flow between GO sheets in the maximum amplitude of velocity in the flow profile. This difference, however, is only quantitative and does not change conclusive arguments on the nature of the confined water flow. Thus, for simplicity, we present here only results with forces applied to all water molecules in the channel. All simulations here were performed after well-converged equilibration at 300 K using the Berendsen thermostat with the temperature calculated after removing the center-of-mass velocity. Recent studies show that thermostating could have a significant effect in the dynamics of strongly driven confined fluid [24]. To measure this effect, we carried out additional simulations with a Nosé-Hoover thermostat applied to the degree of freedom perpendicular to the flow direction and found no significant difference compared to the ones using the Berendsen thermostat [18]. The carbon atoms in GO were frozen in the dynamic simulations to maintain the planar conformation of the GO sheet as stacked in a paper or thin-film form. After the flow is driven, it usually takes a few nanoseconds to reach the steady flow state where the external driving force and friction balance. Our following discussion is based on simulation data collected in the subsequent stages.

III. RESULTS AND DISCUSSION

A. Interfacial slippage

We first explored the interfacial slippage between the water and the GO walls. To quantify it, the solid-liquid friction coefficient λ was calculated from the frictional force autocorrelation function in the equilibrium molecular dynamics (EMD) simulations, following the Green-Kubo formulation,

$$\lambda = \frac{1}{Sk_BT}\int_0^\infty \langle F_x(t)F_x(0)\rangle dt, \tag{1}$$

where $F_x(t)$ is the time-dependent total force acting on the surface with area S, which could then be related to the slip length l_s through $l_s = \eta/\lambda$ [3,7,25,26]. It should be noted that this relation was critiqued for not capturing the intrinsic property of the fluid-solid interface [27], and thus, we performed a comparative study using both EMD and

NEMD simulation methods. A shear viscosity $\eta = 0.729$ mPa s (for the SPC/E water model at 300 K) could be used for the confined water in the evaluation [28]. However, one should be aware that the apparent viscosity of water in our system could be modified by the nanoconfinement [8,29,30]. Thus, further corrections to the apparent viscosity from the interlayer distance between GO sheets should be and was included in our paper for the accurate prediction of λ, which will be discussed later in the text. The results are plotted in Fig. 1(a), which indicate that the slip length of water flow between pristine graphene sheets is 48.13 $\pm$ 4.02 nm and is shortened drastically by two orders to 0.44 $\pm$ 0.12 nm for $c = 30\%$. The slip length for water flow between graphene layers is consistent with the results reported in Refs. [4,5]. As the flow enhancement factor $\varepsilon = 1 + 6l_s/d$ for the Poiseuille flow with interplate distance d, ε is then reduced by two orders as well. Moreover, we also found that the interfacial slip is enhanced as the contact angle θ_c increases. This correlation suggests a direct impact from molecular interaction between water and structures, which is much enhanced in the hydrophilic GO and increases with c because of the electrostatic forces between water and hydroxyl groups. According to Ref. [7], there exists a quasiuniversal relationship between slip length l_s and contact angle θ_c, i.e., $l_s \sim (1 + \cos\theta_c)^{-2}$. In our paper, this scaling relation was reassessed for GO channels with different concentrations of hydroxyl groups. To this end, a relaxation time τ_F was introduced as

$$\tau_F = \int_0^\infty \langle F_x(t)\, F_x(0)\rangle \Big/ \langle F_x^2\rangle dt, \tag{2}$$

which characterizes the decay of force autocorrelation. The results show that τ_F decreases with c as shown in Fig. 2 instead of being a constant as assumed in Ref. [7]. The relationship between l_s and θ_c can be modified and can be rewritten as $l_s/\tau_F \sim (1 + \cos\theta_c)^{-2}$ that can fit our results well for GO. However, this fitting still cannot include our result for water flow between pristine graphene sheets due to the contrastive nature of the interfacial interaction; this issue will be explored in our future paper.

The interfacial slip also was calculated according to the definition of Navier slip length $l_s = v_s/(dv/dz)|_{z=0}$, where v_s is the slip velocity at the fluid-wall interface and dv/dz is the tangent of the velocity profile along the normal direction z. The exact position of the interface ($z = 0$) is defined as the average position of the first water layer from GO sheets. l_s extracted from the velocity profiles in our NEMD simulations is plotted in Fig. 1(b) for different molecular structures and driving forces. Our results show that the NEMD results are consistent with the correlation function based ones in equilibrium for flow between GO sheets (Fig. 3), which suggests the NEMD actually captures the essential fluid dynamics at the interface and the divergence of slip length at a high pressure gradient does not occur [4,5]. This consistency also confirms the significant suppression of water slippage by the presence of hydroxyl groups at a low concentration.

B. The liquid structure of interlayer water

In addition to the interfacial slip, the liquid structure of nanoconfined water also has a strong effect on the molecular

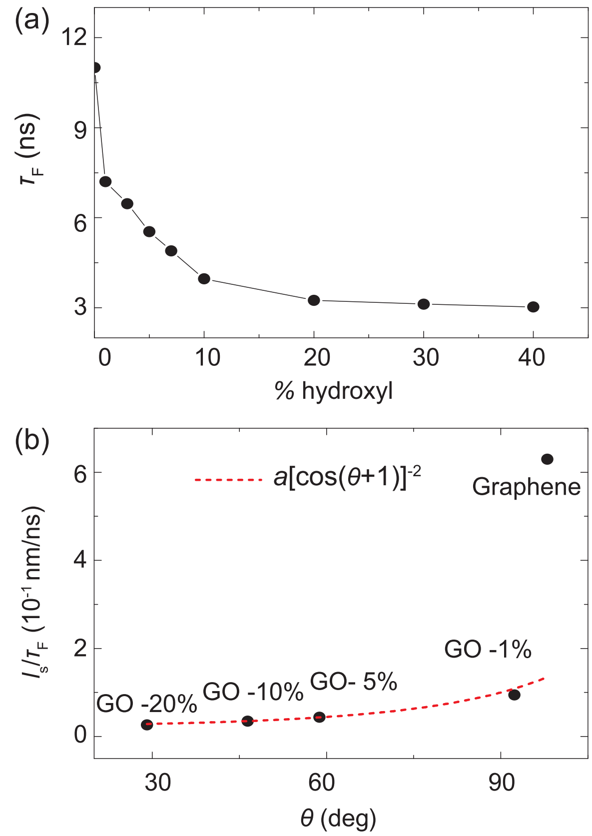

FIG. 2. (Color online) (a) Relationship between relaxation time τ_F and c for $h = 1.7$ nm. (b) The ratio l_s/τ_F plotted against the contact angle θ_c. The results lie on a curve of $l_s/\tau_F = a(1 + \cos\theta_c)^{-2}$ where the fitting parameter is $a = 0.077$.

transport. The subcontinuum transport mechanism in narrow carbon nanotubes recently was pointed out by Falk *et al.* [3] and Thomas and McGaughey [12] and other researchers, who suggested the existence of several low-dimensional ordered forms of structured water in nanochannels, such as the interior

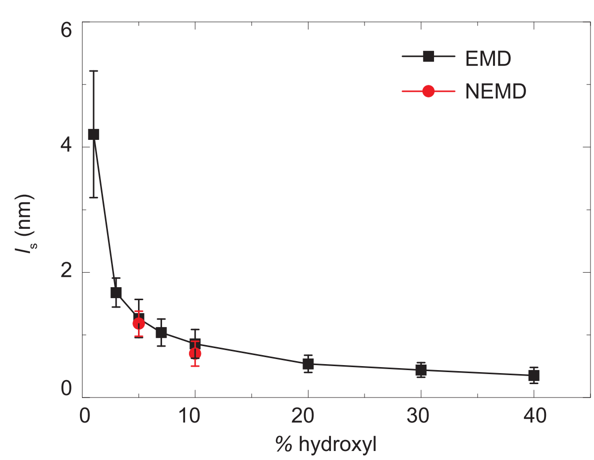

FIG. 3. (Color online) The slip length l_s plotted against hydroxyl concentration c for $h = 1.7$ nm. The square symbols are values of l_s calculated by the Green-Kubo formula in EMD simulations, and the solid circles are from NEMD simulations by fitting the velocity profile.

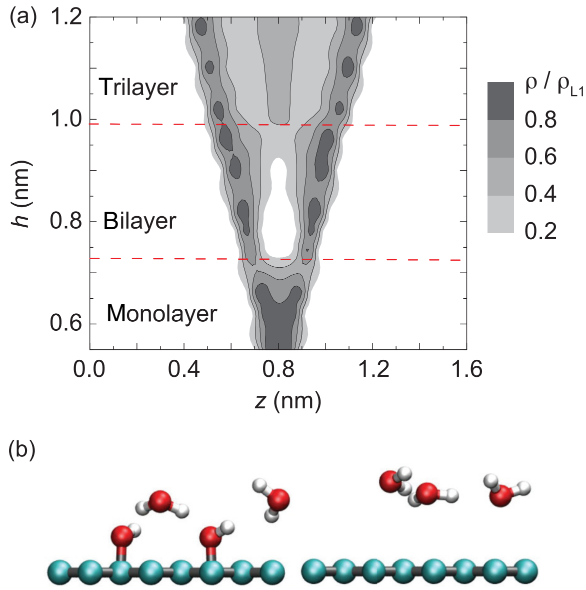

FIG. 4. (Color online) (a) Contour plot of the water density distribution $\rho(z,h)$ between GO at $c = 10\%$ with a reference to the density of the first water layer ρ_{first}. ρ was calculated from MD simulation results for different interlayer distances h, measured from basal planes of GO. The gray level in the plot increases with ρ/ρ_{L1}. (b) Snapshots of the interfacial structures among water molecules, hydroxyl groups, and pristine graphene sheets.

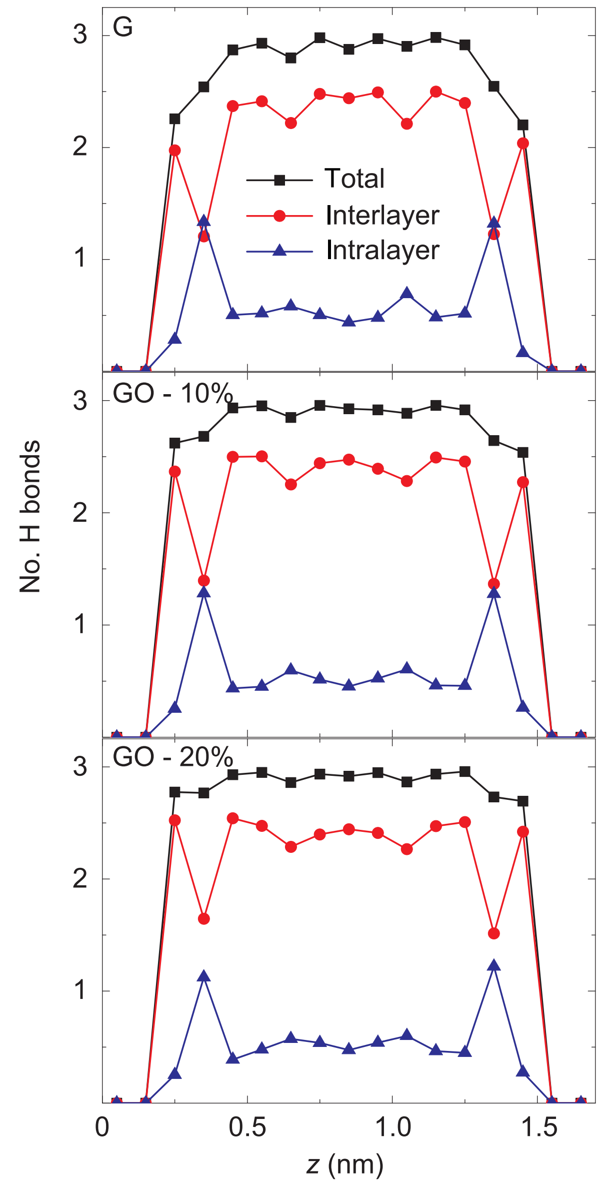

FIG. 5. (Color online) Spatial distribution of the number of hydrogen bonds (H bonds) of each water molecule confined in GO channels with c up to 20%.

space of carbon nanotubes with diameters of ∼1 nm, e.g., wires and nanotubes [10,11]. In comparison, the spatial constriction is much released in the 2D gallery space between graphitic layers. However, contrastive structures of the first few water molecular layers from the sheet are expected. From the spatial density of water molecules calculated from MD simulations, single, bilayer, and trilayer structures of water between graphene sheets are clearly identified [Fig. 4(a)]. For interlayer distance h below 0.7 nm, a water monolayer is observed, with H-bond networks forming with hydroxyl groups on GO. Distinct bilayer and trilayer water structures exist below $h = 1.0$ and 1.4 nm, respectively. With increasing water content, layered order cannot be preserved further, and the liquid structure becomes close to the bulk phase ($h > 3$ nm).

It is interesting to note that, although the hydroxyl groups intercalated between the water and the carbon basal plane in GO, the shorter interacting range of H bonds than van der Waals interactions leads to a similar distance from the basal plane to the first water layer (L1), whether or not the graphene sheet is functionalized [Fig. 4(b)]. This is interesting because the water flow between GO with a certain pattern of oxidation groups can then be considered as a continuum without differences in the geometry but only modification of the boundary slip condition and structures of water confined therein. To further characterize the order of the H-bond network forming between GO sheets, we analyzed the H-bond network structures and categorized H bonds into intralayer and interlayer contributions (the layers are defined with thicknesses of 0.1 nm). Moreover, in L1 (with an average distance of ∼0.35 nm from the basal plane), water molecules prefer to lie in parallel to the basal plane in the pristine graphene region, corresponding to a peak in the intralayer H-bond distribution (Fig. 5). For the water molecules further from the GO sheet, a more random distribution is identified for their orientations with the number of intralayer H bonds per water molecule equaling ∼1/3 of the peak value for L1. On the other hand, as c increases, more H bonds could form between the water molecules in L1 and the GO sheets, thus, the peak in the intralayer H-bond distribution is reduced, and the amplitude of distribution in interlayer H bonds increases. Our simulation results indicate further that the interlayer distance does not modify these structural characteristics. As the nanoconfined water flow between GO sheets critically depends on the first few water layers from GO sheets, which provide the boundary condition for the flow profile, flow characteristics that deviate from bulk water flow would be expected.

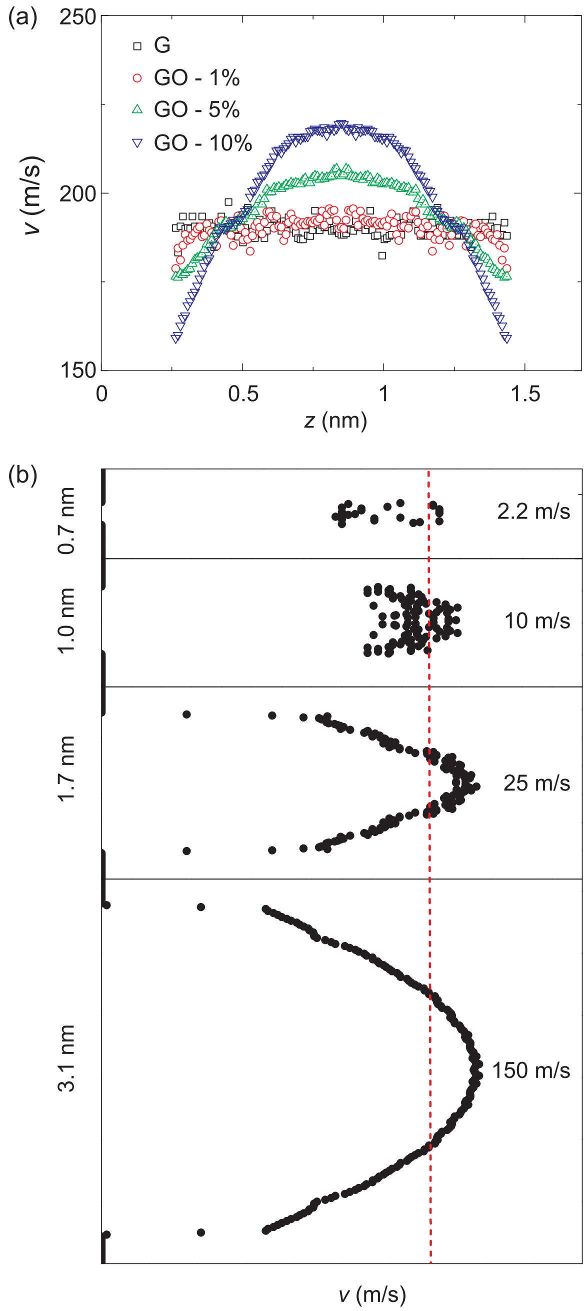

FIG. 6. (Color online) (a) Flow velocity profiles of water at different concentrations of hydroxyl groups on the graphene sheet with $h = 1.7$ nm. (b) Effects of the interlayer distance h on the flow behavior for $c = 10\%$ and $\mathrm{d}p/\mathrm{d}x = 68.5$ MPa/nm. The red dashed lines indicate a base value as annotated for each subplot.

C. The viscous nature of flow

With the hydroxyl functionalization on graphene, not only the interfacial slip is suppressed as measured for the reduction in l_s, the nature of the flow is also modified. To characterize this, we plotted the flow profiles of water in Fig. 6(a). It is clearly shown that, in contrast to the flow between graphene layers, the velocity profile for flow between GO sheets changes from a "plateau" with very low curvature ($c < 1\%$) to a parabolic one at high c values. The trend is even more significant as c increases. The nanoconfinement reshapes the profile further. Parabolic viscous flow characteristics are recovered for $c = 10\%$ [Fig. 6(b)], although there are discrete data points deviating from the ideal behavior for h below 1.0 nm. The breakdown of slip flow by increasing surface functionalization or releasing the nanoconfinement (increasing h) is found to be continuous instead of transitional, similar to the changes observed in interfacial slippage and friction.

The parabolicity of the velocity profile implies that continuum hydrodynamics could apply. The viscous flow between parallel plates can be captured by the Poiseuille solution of the Navier-Stokes equations,

$$Q = -(\mathrm{d}p/\mathrm{d}x)\, d^3/12\eta, \tag{3}$$

where Q is the flow rate and $\mathrm{d}p/\mathrm{d}x$ is the pressure gradient along the flow direction x. In calculating the pressure, we added corrections to the cross-sectional area by excluding the depletion layer at the boundaries, and d is redefined as the effective thickness where the water-free region ($\sim$0.5 nm in total) from the basal plane is excluded as well. We plot Q against d at a constant $\mathrm{d}p/\mathrm{d}x$ from 20.0 to 100.0 Pa/nm in Fig. 7(a). The results show that the scaling relation between

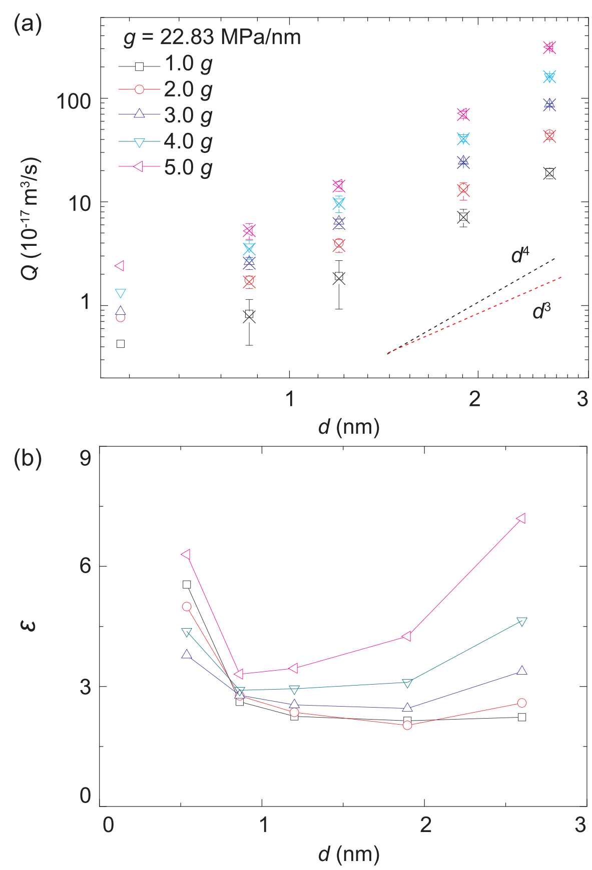

FIG. 7. (Color online) (a) Flow rate Q predicted from Poiseuille law with corrections on both the apparent viscosity and the boundary slip [Eq. (4)] (cross), compared with the simulation results (open symbols) with effective interlayer distance d at the hydroxyl groups' concentration of $c = 10\%$. The pressure gradient is expressed in units of $g = 22.83$ MPa/nm. Data points for $d = 0.54$ nm are not available for prediction because of the absence of parabolic profile (water bilayer forms). (b) Flow enhancement factor ε as a function of d.

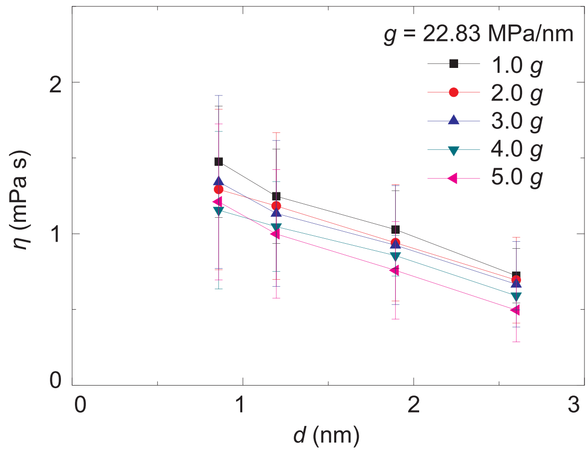

FIG. 8. (Color online) The apparent viscosity of nanoconfined water flow as a function of the effective distance d, calculated at a different pressure gradient of $g = 22.83$ MPa/nm.

Q and d deviates from cubic ($Q \sim d^3$) towards quartic ($Q \sim d^4$). This can be explained by the reduction in η as d increases, which can be evaluated by fitting the velocity profile to the Poiseuille law (Fig. 8). It should be noticed that this η-d dependence follows the same trend with other hydroxyl-containing surfaces but contradicts with that observed for water in carbon nanotubes [8,29–31], which may be correlated to their hydrophobicity.

From the Q-d dependence, we quantified the flow enhancement parameter $\varepsilon = \gamma/\gamma_{\text{no slip}}$, where the hydraulic conductivity γ and $\gamma_{\text{no slip}}$ were calculated from MD simulations, i.e., $\gamma = v/(\mathrm{d}p/\mathrm{d}x)$ and Eq. (3), respectively. The results shown in Fig. 7(b) were calculated by using the bulk viscosity of water, which shows that ε first decreases and then increases with d. In comparison with bulk water flow that can be described by the Poiseuille law, high values of γ at small and large d (<3 nm), correspond to the enhancement by interfacial slip and reduction in viscosity, respectively.

The apparent viscosity η of water confined in the GO channel was estimated by fitting the velocity profiles to predictions from Poiseuille flow. The results show that η decreases as d increases. The dependence between flux rates Q and d is reassessed by including: (1) the modified η and (2) the slip boundary condition in the Poiseuille law. We see that the MD results agree well with this corrected prediction and, thus, conclude that the water flow in the GO channel is viscous.

The enhancement factor ε was estimated with the modified apparent viscosity. The contributions from apparent viscosity and boundary slip are estimated separately. First, we use the modified η to calculate $\gamma_{\text{no slip}}$ [Fig. 9(a)] and then deduce the slip flow contribution from simulation results in evaluating γ [Fig. 9(b)]. By adding corrections from apparent viscosity and interfacial slip, we found that the flow enhancement is majorly contributed by the interfacial slippage, whereas, the effect of reduced viscosity becomes important only at large d (Fig. 7). The enhancement increases with the pressure gradient in the latter mechanism as well. The slip boundary condition could finally be incorporated into the hydrodynamics, yielding

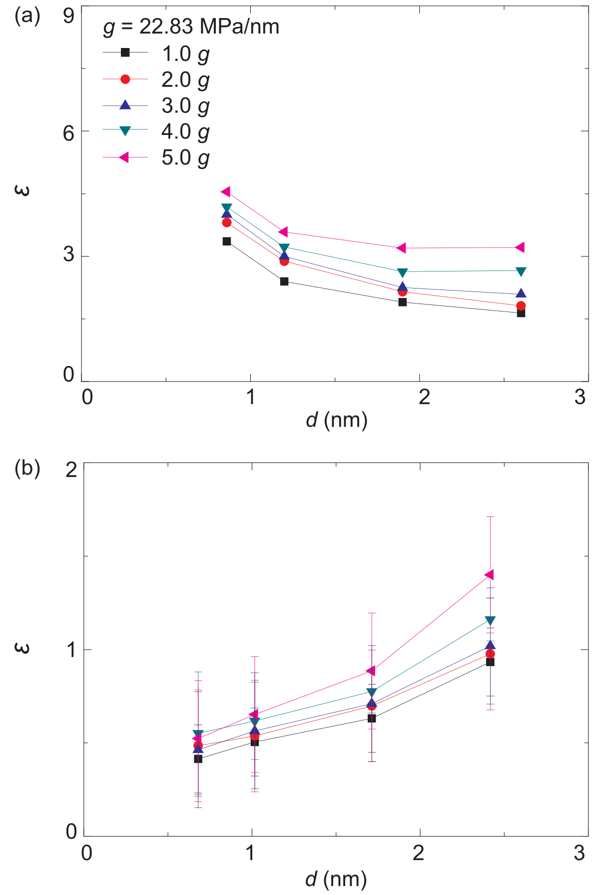

FIG. 9. (Color online) Flow enhancement ε as a function of d with corrections on the apparent viscosity η. In panel (b), the flow rate due to boundary slip is deduced from the simulation results in evaluating γ.

a modified prediction for Q,

$$Q = -(1 + 6\eta/\beta d)(\mathrm{d}p/\mathrm{d}x)\, d^3/12\eta, \tag{4}$$

where $\beta = -(\mathrm{d}p/\mathrm{d}x)d/2v_s$ and the enhancement by slip is the second term. By using the modified values of η, Eq. (4) could perfectly predict the water flow between GO sheets from the MD simulations [Fig. 8(a)], confirming that the essential physics is correctly captured in the model.

D. Correspondence between EMD and NEMD simulations

As mentioned in Sec. IIIA, we identified consistence in the prediction of slip lengths using EMD and NEMD simulations. It was critiqued by Petrovic and Harrowell [27] that the Green-Kubo approach fails to yield the correct Navier friction coefficient. To clarify this point, we further explored the correspondence between EMD and NEMD simulations for $c = 10\%$ and h ranging from 1.36 to 3.1 nm. The results, as shown in Fig. 10, clearly show quantitative consistence between these two approaches, i.e., the difference in results is close to the error measured over independent runs of simulations using the same method. Moreover, with the corrections on the apparent viscosity made, both methods predict the same h dependence, i.e., the slip length decreases with the interlayer distance, in contradiction with the argument in Ref. [27] that the slip

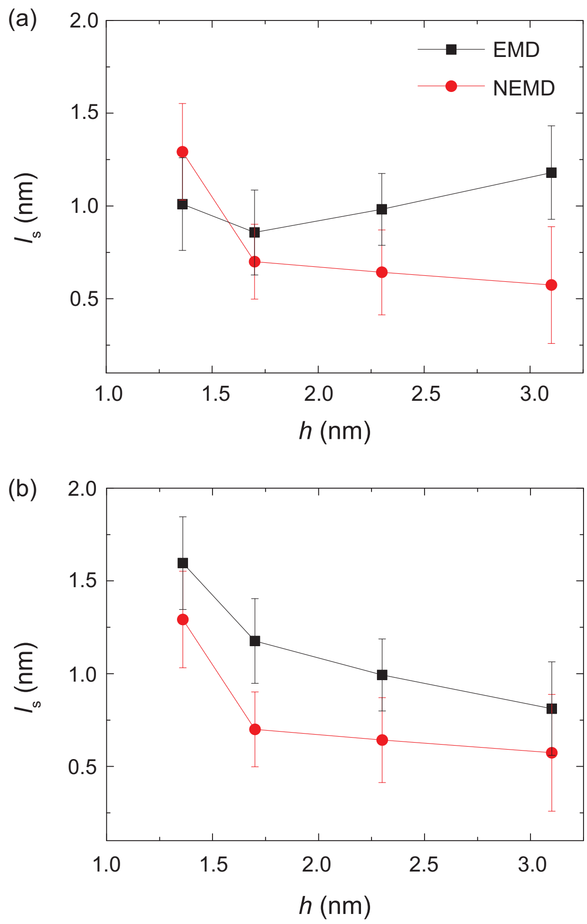

FIG. 10. (Color online) Slip lengths calculated from EMD and NEMD simulations for $c = 10\%$ without (a) and with (b) corrections on the apparent viscosity.

length is an intrinsic property of the interface and should be independent of the wall separation. Although further work by including the effects of the interfacial structures, flow setup (Couette, etc.), and rate should be performed for a rigorous discussion on this correspondence, our simulation results here are sufficient to validate our calculations of slip lengths and relevant discussion on the nature of nanoconfined flow between graphene oxides.

IV. CONCLUSION

To summarize, we revealed the breakdown of fast slip flow in chemically functionalized graphene sheets, which could be weakened further by relaxing the nanoconfinement. MD simulation results show that hydrodynamics applies even at scales down to nanometers in this regime, but corrections on the slip boundary condition and apparent viscosity of nanoconfined liquid must be included. The contrastive nature from flow between pristine graphene arises from the electrostatic contribution to the interfacial interaction and the modification of H-bond networks. Recent experiments showed that the structure of GO is influenced strongly by the humidity where over 70% expansion in the stacking direction of GO sheets was observed [13,32–34]. Thus, with controlled oxidation and reduction processes in fabricating GO, the conclusion from this computational study could, thus, be verified experimentally.

ACKNOWLEDGMENTS

This work was supported by the National Natural Science Foundation of China through Grants No. 11222217, No. 11002079, and No. 21271154 and the Tsinghua University Initiative Scientific Research Program No. 2011Z02174. This work was performed on the Explorer 100 cluster system of the Tsinghua National Laboratory for Information Science and Technology.

[1] M. Majumder, N. Chopra, R. Andrews, and B. J. Hinds, Nature (London) **438**, 44 (2005).
[2] J. K. Holt, H. G. Park, Y. M. Wang, M. Stadermann, A. B. Artyukhin, C. P. Grigoropoulos, A. Noy, and O. Bakajin, Science **312**, 1034 (2006).
[3] K. Falk, F. Sedlmeier, L. Joly, R. R. Netz, and L. Bocquet, Nano Lett. **10**, 4067 (2010).
[4] S. K. Kannam, B. D. Todd, J. S. Hansen, and P. J. Daivis, J. Chem. Phys. **135**, 144701 (2011).
[5] S. K. Kannam, B. D. Todd, J. S. Hansen, and P. J. Daivis, J. Chem. Phys. **138**, 094701 (2013).
[6] A. Siria, P. Poncharal, A.-L. Biance, R. Fulcrand, X. Blase, S. T. Purcell, and L. Bocquet, Nature (London) **494**, 455 (2013).
[7] D. M. Huang, C. Sendner, D. Horinek, R. R. Netz, and L. Bocquet, Phys. Rev. Lett. **101**, 226101 (2008).
[8] J. A. Thomas and A. J. H. McGaughey, Nano Lett. **8**, 2788 (2008).
[9] S. Joseph and N. R. Aluru, Nano Lett. **8**, 452 (2008).
[10] K. Koga, G. T. Gao, H. Tanaka, and X. C. Zeng, Nature (London) **412**, 802 (2001).
[11] J. Bai, J. Wang, and X. C. Zeng, Proc. Natl. Acad. Sci. U.S.A. **103**, 19664 (2006).
[12] J. A. Thomas and A. J. H. McGaughey, Phys. Rev. Lett. **102**, 184502 (2009).
[13] R. R. Nair, H. A. Wu, P. N. Jayaram, I. V. Grigorieva, and A. K. Geim, Science **335**, 442 (2012).
[14] S. Kim, S. Zhou, Y. Hu, M. Acik, Y. J. Chabal, C. Berger, W. de Heer, A. Bongiorno, and E. Riedo, Nat. Mater. **11**, 544 (2012).
[15] D. R. Dreyer, S. Park, C. W. Bielawski, and R. S. Ruoff, Chem. Soc. Rev. **39**, 228 (2010).
[16] S. Plimpton, J. Comp. Phys. **117**, 1 (1995).
[17] C.-J. Shih, S. Lin, R. Sharma, M. S. Strano, and D. Blankschtein, Langmuir **28**, 235 (2011).
[18] W. Xiong, J. Z. Liu, M. Ma, Z. Xu, J. Sheridan, and Q. Zheng, Phys. Rev. E **84**, 056329 (2011).
[19] T. Werder, J. H. Walther, R. L. Jaffe, T. Halicioglu, and P. Koumoutsakos, J. Phys. Chem. B **107**, 1345 (2003).
[20] J. Rafiee, X. Mi, H. Gullapalli, A. V. Thomas, F. Yavari, Y. Shi, P. M. Ajayan, and N. A. Koratkar, Nat. Mater. **11**, 217 (2012).
[21] R. W. Hockney and J. W. Eastwood, *Computer Simulation Using Particles* (Taylor & Francis, New York, 1989).
[22] P. Sun, M. Zhu, K. Wang, M. Zhong, J. Wei, D. Wu, Z. Xu, and H. Zhu, ACS Nano **7**, 428 (2013).

[23] C. Chen, M. Ma, K. Jin, J. Z. Liu, L. Shen, Q. Zheng, and Z. Xu, Phys. Rev. E **84**, 046314 (2011).
[24] S. Bernardi, B. D. Todd, and D. J. Searles, J. Chem. Phys. **132**, 244706 (2010).
[25] L. Bocquet and J.-L. Barrat, Phys. Rev. E **49**, 3079 (1994).
[26] L. Bocquet and J.-L. Barrat, J. Chem. Phys. **139**, 044704 (2013).
[27] J. Petravic and P. Harrowell, J. Chem. Phys. **127**, 174706 (2007).
[28] M. A. Gonzalez and J. L. F. Abascal, J. Chem. Phys. **132**, 096101 (2010).
[29] X. Chen, G. Cao, A. Han, V. K. Punyamurtula, L. Liu, P. J. Culligan, T. Kim, and Y. Qiao, Nano Lett. **8**, 2988 (2008).
[30] N. R. Haria, G. S. Grest, and C. D. Lorenz, J. Phys. Chem. C **117**, 6096 (2013).
[31] P. J. Feibelman, J. Phys. Chem. C **117**, 6088 (2013).
[32] D. A. Dikin, S. Stankovich, E. J. Zimney, R. D. Piner, G. H. B. Dommett, G. Evmenenko, S. T. Nguyen, and R. S. Ruoff, Nature (London) **448**, 457 (2007).
[33] A. Buchsteiner, A. Lerf, and J. Pieper, J. Phys. Chem. B **110**, 22328 (2006).
[34] A. Lerf, H. He, M. Forster, and J. Klinowski, J. Phys. Chem. B **102**, 4477 (1998).